IEEE Access
Multidisciplinary | Rapid Review | Open Access Journal

Received April 22, 2021, accepted June 9, 2021, date of publication July 19, 2021, date of current version September 7, 2021.

Digital Object Identifier 10.1109/ACCESS.2021.3098319

Thermal Modeling and Experimental Validation in the Rotor Region of Hydrogenerator With Different Rotor Structures

HAN JICHAO[1], LIU YUFEI[1], DONG JIECHEN[1], SUN YUTIAN[2,3,4], GE BAOJUN[1], AND LI WEILI[1]

[1]School of Electrical and Electronic Engineering, Harbin University of Science and Technology, Harbin 150080, China
[2]State Key Laboratory of Hydro-Power Equipment, Harbin 150040, China
[3]Harbin Electric Machinery Company Ltd., Harbin 150040, China
[4]Harbin Institute of Large Electrical Machinery, Harbin 150040, China

Corresponding author: Han Jichao (hanjichao163@163.com)

This work was supported in part by the National Natural Science Foundation of China under Grant 52177037, in part by the National Natural Science Foundation of China under Grant 51807043, in part by the Natural Science Foundation of Heilongjiang Province of China under Grant YQ2021E037, in part by the Fundamental Research Foundation for Universities of Heilongjiang Province under Grant 2019-KYYWF-0209, in part by the Postdoctoral Foundation of Heilongjiang Province of China under Grant LBH-TZ1005, in part by the China Postdoctoral Science Foundation under Grant 2018T110269, in part by the China Postdoctoral Science Foundation under Grant 2018M630336, in part by the Fundamental Research Foundation for Universities of Heilongjiang Province under Grant 2018-KYYWF-1629, in part by the Postdoctoral Foundation of Heilongjiang Province of China under Grant LBH-Z17040, and in part by the Research Foundation of State Key Laboratory of Hydro-power Equipment under Grant SKLHE-ORF-202001.

ABSTRACT Thermal management is often considered a bottleneck in the pursuit of the next generation hydrogenerator in the electric power system. Overheating of the complex rotor parts has become one of the main problems affecting safe and stable hydrogenerator operation. In this paper, a 250 MW hydrogenerator is analyzed. The transient electromagnetic field of the hydrogenerator is calculated and the losses of the rotor parts are obtained. The rotation of the hydrogenerator rotor is considered. Three-dimensional fluid and thermal mathematic and physical models of the hydrogenerator are established. The loss values from electromagnetic field calculations are applied to the rotor parts as heat sources in the temperature field. After solving the fluid and thermal equations of fluid-solid conjugated heat transfer, influence of the structures of rotor support plate, rotor pole body insulation, and rotor excitation winding on the fluid flow and temperature distribution in the rotor region of hydrogenerator is studied using the finite volume method. The calculated temperature result of rotor excitation winding is compared with the measured value. The calculated temperature result agrees well with the measured value. It provides an important reference for optimizing the rotor structure of the larger hydrogenerator.

INDEX TERMS Hydrogenerator, different rotor structures, rotor rotation, transient electromagnetic field, fluid flow, temperature distribution.

I. INTRODUCTION

As a key energy conversion equipment in the electric power system, the safety and stability of hydrogenerator are very important. With the capacity increase of the hydrogenerator, overheating problem of hydrogenerator become more and more serious. Because the current of the rotor excitation winding is high, it results in the high temperature of the rotor excitation winding in the hydrogenerator. The structures of rotor support plate, rotor pole body insulation, and rotor excitation winding could affect obviously the temperature of the rotor region in the hydrogenerator. Reasonable rotor structure design could reduce the temperature of rotor parts in the rotor region.

In recent years, researchers have extensively focused on the physical field in the hydrogenerator. For example, Meiswinkel *et al.* performed transient Roebel bar force calculation in large salient-pole hydrogenerators. Carounagarane *et al.* analyzed on thermal behavior of large hydrogenerators operating with continuous overloads [2]. Øyvang *et al.* performed the online model-based thermal prediction for flexible control of an air-cooled hydrogenerator [3]. Dirani *et al.* researched the rotor interturn short circuit impact on large hydrogenerator magnetic quantities [4].

The associate editor coordinating the review of this manuscript and approving it for publication was Su Yan.

This work is licensed under a Creative Commons Attribution 4.0 License. For more information, see https://creativecommons.org/licenses/by/4.0/

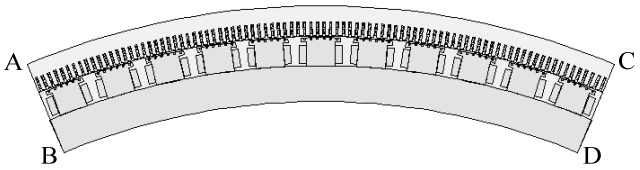

FIGURE 1. Solving region of the transient electromagnetic field in the hydrogenerator.

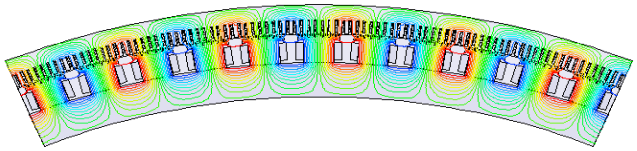

FIGURE 2. Flux distribution of this hydrogenerator.

Valavi performed the electromagnetic analysis and electrical signature-based detection of rotor inter-turn faults in salient-pole synchronous machine [5]. Akiror *et al.* studied the challenges in modeling of large synchronous machines [6]. Gbégbé *et al.* performed the damper currents simulation of large hydro-generator using the combination of FEM and coupled circuits models [7]. Schrittwieser *et al.* analyzed on temperature distribution in the stator of large synchronous machines considering heat conduction and heat convection [8]. Some other experts extensively studied hydrogenerator [9], [10], but very few focused on the influence of rotor structure on the fluid flow and temperature distribution in the rotor region of hydrogenerator.

In this paper, a 250 MW hydrogenerator is analyzed. The transient electromagnetic field of the hydrogenerator is calculated and the losses of the rotor parts are obtained. The rotation of the hydrogenerator rotor is considered. Three-dimensional fluid and thermal mathematic and physical models of the hydrogenerator are established. The loss values from electromagnetic field calculations are applied to the rotor parts as heat sources in the temperature field. After solving the fluid and thermal equations of fluid-solid conjugated heat transfer, influence of the structures of rotor support plate, rotor pole body insulation, and rotor excitation winding on the fluid flow and temperature distribution in the rotor region of hydrogenerator is studied using the finite volume method. This paper provides an important reference for the reasonable design of rotor structure in the larger hydrogenerator.

II. ANALYSIS OF TRANSIENT ELECTROMAGNETIC FIELD

Based on classical electromagnetic theory, mathematical and physical models of the transient electromagnetic field in the hydrogenerator are established [11]. Fig. 1 shows the solving region of the transient electromagnetic field in the hydrogenerator.

Fig. 2 shows the flux distribution of this hydrogenerator. The loss of the rotor exciting winding is 558.1 kW in the rotor region of hydrogenerator. The loss of the rotor magnetic pole surface is caused by the tooth harmonic magnetic field.

FIGURE 3. 250MW hydrogenerator unit.

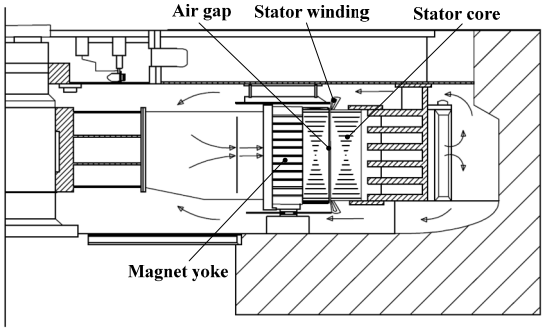

FIGURE 4. Ventilation cooling system of 250MW hydrogenerator.

TABLE 1. Additional loss in the rotor region of hydrogenerator.

	P_{2vk}(kW)	P_{FeP}(kW)	P_{kv}(kW)
Calculated results	44.78	190.75	9.13
Design values	42.535	194.05	—

It includes: (1) Additional loss P_{2vk} caused by harmonic MMF of stator teeth on the surfaces of the rotor magnetic pole and rotor damper bar. (2) Additional loss P_{Fep} of the rotor magnetic pole surface under no-load rated voltage. (3) Rotor surface loss P_{kv} caused by the stator windings MMF harmonic. Table 1 shows the additional loss in the rotor region of hydrogenerator.

III. FLUID-THERMAL COUPLING ANALYSIS MODEL OF HYDROGENERATOR

Fig. 3 shows 250MW hydrogenerator unit. Fig. 4 shows the ventilation cooling system of 250 MW hydrogenerator. Table 2 gives the basic parameters of hydrogenerator. According to the actual structure of 250 MW hydrogenerator, 3-D fluid and thermal coupling analysis model of the hydrogenerator rotor region is established, as shown in Fig. 5.

Fig. 5(a) shows the solving region of hydrogenerator rotor. Fig. 5(b) shows the rotor structure of hydrogenerator. It includes the rotor yoke, rotor ventilation ducts, rotor excitation winding, rotor support plate, rotor pole body, rotor pole body insulation, rotor press plate, and rotor end ring, etc. In the 3-D fluid and thermal coupling analysis model of the hydrogenerator rotor region, fluid velocity of the rotor region inlet is 2 m/s under the rated operating condition. The fluid

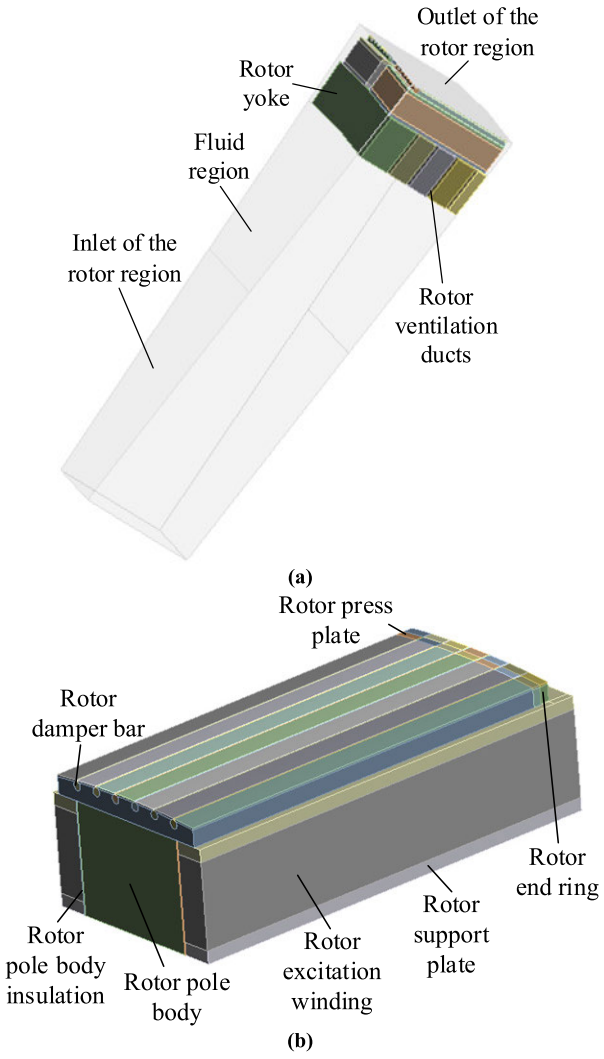

FIGURE 5. 3-D fluid and thermal coupling analysis model of the hydrogenerator rotor region. (a) Solving region. (b) Rotor structure.

TABLE 2. Basic parameters of hydrogenerator.

Rated power	250 MW	Number of poles	88
Outer diameter of rotor	16580m m	Frequency	50Hz
Width of rotor ventilation ducts	32mm	Number of rotor ventilation ducts	9

temperature of the rotor region inlet is 40°C. Rated rotation speed of the rotor is 68.2r/min.

In the 250 MW hydrogenerator rotor region, fluid flow and heat transfer satisfy the laws of mass conservation, momentum conservation, and energy conservation [12]–[17]. The mathematical equations of 3-D fluid and thermal coupling field in the rotor region of hydrogenerator are given as follows.

The law of mass conservation is expressed as follows:

$$\frac{\partial \rho}{\partial t} + \nabla \cdot (\rho \vec{v}) = 0 \tag{1}$$

where $\vec{v}$ is velocity vector, t is time, and ρ is fluid density.

The law of momentum conservation is expressed as follows:

$$\frac{\partial}{\partial t}(\rho \vec{v}) + \nabla \cdot (\rho \vec{v}\vec{v}) = -\nabla p + \nabla \cdot (\bar{\bar{\tau}}) + \rho \vec{g} + \vec{F} \tag{2}$$

where p is static pressure, $\bar{\bar{\tau}}$ is stress tensor, $\rho \vec{g}$ and $\vec{F}$ are gravitational body force, and external body forces, respectively.

The stress tensor $\bar{\bar{\tau}}$ is expressed as follows:

$$\bar{\bar{\tau}} = \mu \left[\left(\nabla \vec{v} + \nabla \vec{v}^T \right) - \frac{2}{3} \nabla \cdot \vec{v} I \right] \tag{3}$$

where μ is the molecular viscosity, I is the unit tensor, and the second term on the right side denotes the effect of volume dilation.

The law of energy conservation is expressed as follows:

$$\frac{\partial}{\partial t}(\rho E) + \nabla \cdot (\vec{v}(\rho E + p)) = \nabla \cdot (k_{eff} \nabla T - \sum_j h_j \vec{J}_j + (\bar{\bar{\tau}}_{eff} \cdot \vec{v})) + S_h \tag{4}$$

where k_{eff} is the effective conductivity, $\vec{J}_j$ is the diffusion flux of species, j the first three terms on the right side of Equation (4) represent energy transfer due to conduction, species diffusion, and viscous dissipation, respectively. S_h includes the heat of chemical reaction and any other volumetric heat sources.

For the Reynolds number larger than 2300, the fluid is turbulent. In this paper, turbulence is simulated with the standard k-ε model. Boltzmann equation with kinetic energy of turbulence k and diffusion factor ε is used in the turbulence model as follows:

$$\begin{cases} \dfrac{\partial}{\partial t}(\rho k) + \mathrm{div}(\rho k \boldsymbol{u}) = \mathrm{div}\left[\left(\mu + \dfrac{\mu_t}{\sigma_k} \right) \mathbf{grad} k \right] \\ + G_k - \rho \varepsilon \\ \dfrac{\partial}{\partial t}(\rho \varepsilon) + \mathrm{div}(\rho \boldsymbol{u} \varepsilon) = \mathrm{div}\left[\left(\mu + \dfrac{\mu_t}{\sigma_\varepsilon} \right) \mathbf{grad} \varepsilon \right] \\ + G_{1\varepsilon} \dfrac{\varepsilon}{k} G_k - G_{2\varepsilon} \rho \dfrac{\varepsilon^2}{k} \end{cases} \tag{5}$$

where G_k is the generation rate of the turbulence, μ_t is the turbulent viscosity coefficient, $G_{1\varepsilon}$, $G_{2\varepsilon}$ are constants and σ_k, σ_ε are Planck constants.

IV. INFLUENCE OF ROTOR STRUCTURE ON THE FLUID FLOW AND TEMPERATURE DISTRIBUTION IN THE ROTOR REGION OF HYDROGENERATOR

The structures of the rotor support plate, rotor pole body insulation, and rotor excitation winding affect directly fluid flow between the rotor magnetic poles and temperature of the rotor excitation winding. During the heat transfer and fluid flow calculations in the rotor region of hydrogenerator, loss values obtained from transient electromagnetic field calculation with different rotor structures are applied to the rotor parts as heat source. The rotation of the hydrogenerator rotor is considered. After solving the fluid and thermal equations

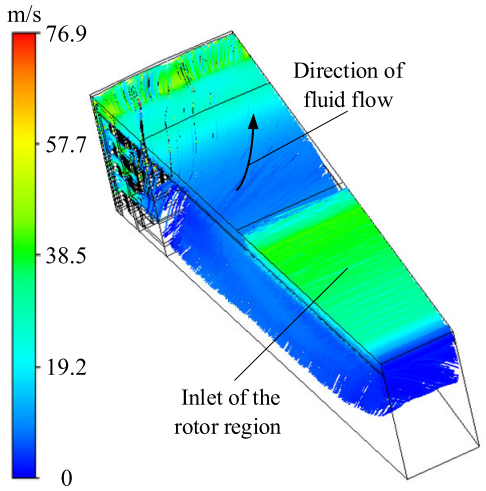

FIGURE 6. Streamline of fluid flow in the rotor region of hydrogenerator when the width of the rotor support plate reduces by 5mm.

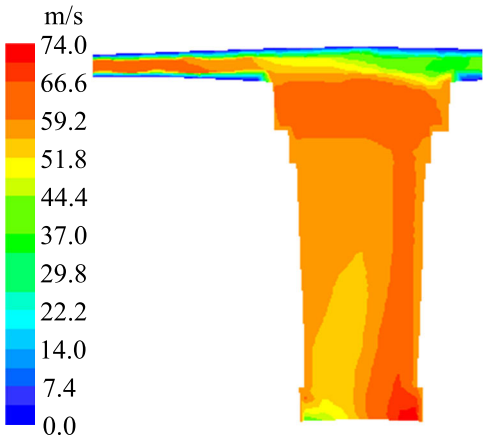

FIGURE 7. Fluid velocity distribution when the width of the rotor support plate reduces by 5mm.

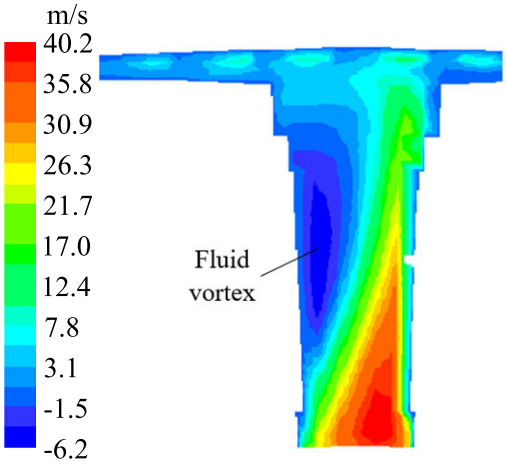

FIGURE 8. Radial fluid velocity distribution when the width of the rotor support plate reduces by 5mm.

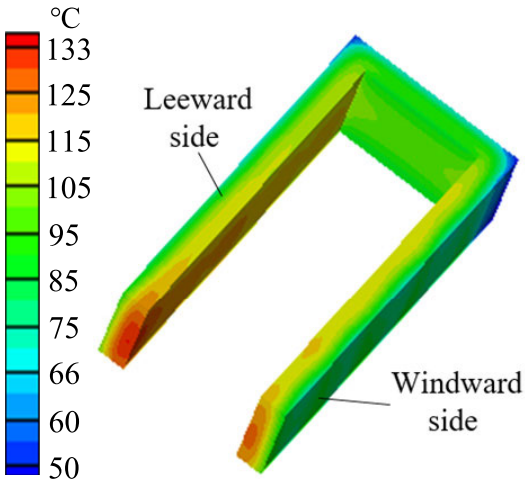

FIGURE 9. Temperature distribution of rotor excitation winding.

of fluid–solid conjugated heat transfer, influence of the width of rotor support plate, the thickness of rotor pole body insulation, and the width of the rotor excitation winding on the fluid flow and temperature distribution in the rotor region of hydrogenerator is determined [18]–[22].

A. INFLUENCE OF THE WIDTH OF THE ROTOR SUPPORT PLATE ON FLUID VELOCITY AND TEMPERATURE IN THE ROTOR REGION OF HYDROGENERATOR

Fig. 6 shows the streamline of fluid flow in the rotor region of hydrogenerator. The rotor rotation of the hydrogenerator drives the fluid flow in the rotor region. The highest fluid velocity in the rotor region is 76.9m/s when the width of the rotor support plate reduces by 5mm.

Figs. 7 and 8 show the distribution of fluid velocity and radial fluid velocity between the rotor magnetic poles when the width of the rotor support plate reduces by 5mm. It can be seen from Fig. 7 that the highest fluid velocity is 74m/s in this section when the width of the rotor support plate reduces by 5mm. In the rotor region of hydrogenerator, fluid velocity in the radial direction plays a major role in cooling the rotor excitation winding. Fig. 7 shows that the highest fluid velocity is 40.2m/s in this section when the width of the rotor support plate reduces by 5mm. The highest radial fluid velocity is 1.4m/s lower than that under the original structure. Fluid vortex appears between the rotor magnetic poles.

Fig. 9 shows the temperature distribution of rotor excitation winding when the width of the rotor support plate reduces by 5mm. The highest temperature of the rotor excitation winding is 133°C and appears on the leeward side. It is 1°C higher than that of the rotor excitation winding on the leeward side under the original structure. The highest temperature of the rotor excitation winding is 125°C on the windward side. It is 2°C higher than that of the rotor excitation winding on the windward side under the original structure. Fig. 10 gives the isotherm of rotor excitation winding. The temperature of rotor excitation winding on the leeward is higher than that of rotor excitation winding on the windward side. The temperature difference of rotor excitation winding on the leeward side and on the windward side is 8°C.

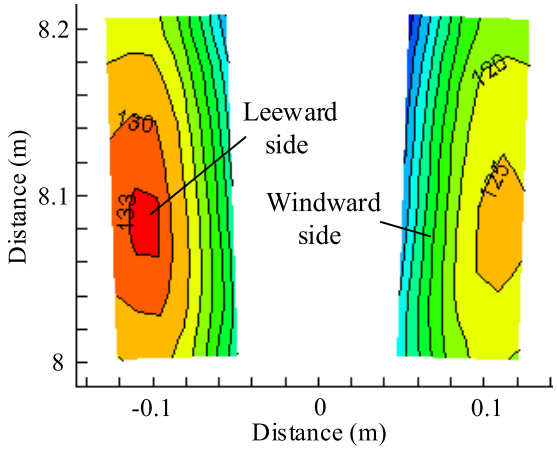

FIGURE 10. Isotherm of rotor excitation winding.

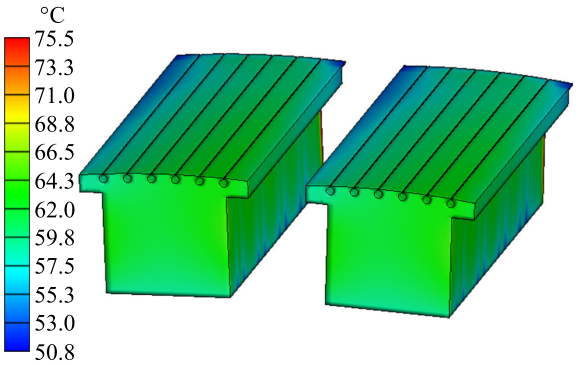

FIGURE 11. Temperature distribution of rotor pole body.

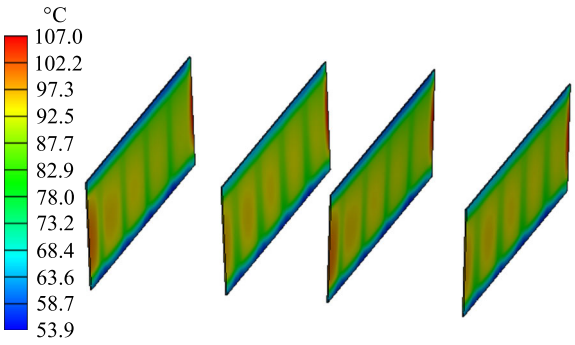

FIGURE 12. Temperature distribution of rotor pole body insulation.

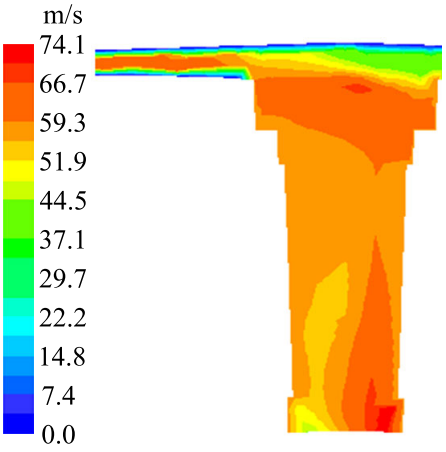

FIGURE 13. Fluid velocity distribution when the width of the rotor support plate reduces by 5mm.

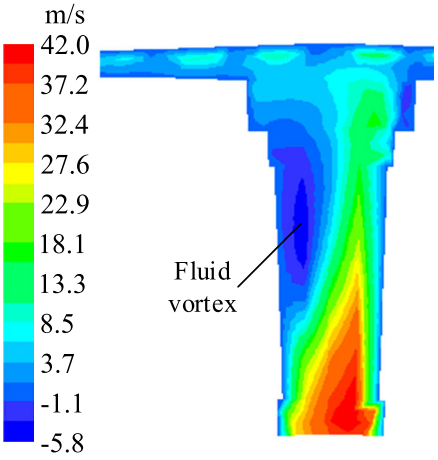

FIGURE 14. Radial fluid velocity distribution when the width of the rotor support plate reduces by 5mm.

Figs. 11 and 12 give the temperature distribution of rotor pole body and rotor pole body insulation. The highest temperature of rotor pole body and rotor pole body insulation is 75.5°C and 107°C when the width of the rotor support plate reduces by 5mm, respectively. Rotor pole body insulation contacts with the rotor excitation winding. It results in the high temperature of rotor pole body insulation.

B. INFLUENCE OF THE THICKNESS OF THE ROTOR POLE BODY INSULATION ON THE FLUID VELOCITY AND TEMPERATURE IN THE ROTOR REGION OF HYDROGENERATOR

Figs. 13 and 14 show the distribution of fluid velocity and radial fluid velocity between the rotor magnetic poles when the thickness of rotor pole body insulation increases by 5mm. It can be seen from Fig. 13 that the highest fluid velocity is 74.1m/s in this section. Fig. 14 shows the highest radial fluid velocity is 42m/s in this section when the thickness of rotor pole body insulation increases by 5mm. The highest radial fluid velocity is 0.4m/s higher than that under the original structure.

Fig. 15 shows the temperature distribution of rotor excitation winding when the thickness of rotor pole body insulation increases by 5mm. The highest temperature of the rotor excitation winding is 138°C and appears on the leeward side. It is 6°C higher than that of the rotor excitation winding on the leeward side under the original structure. The highest temperature of the rotor excitation winding is 135°C on the windward side. It is 12°C higher than that of the rotor excitation winding on the windward side under the original structure. Fig. 16 gives the isotherm of rotor excitation winding. The temperature difference of rotor excitation winding on the leeward side and on the windward side is 3°C.

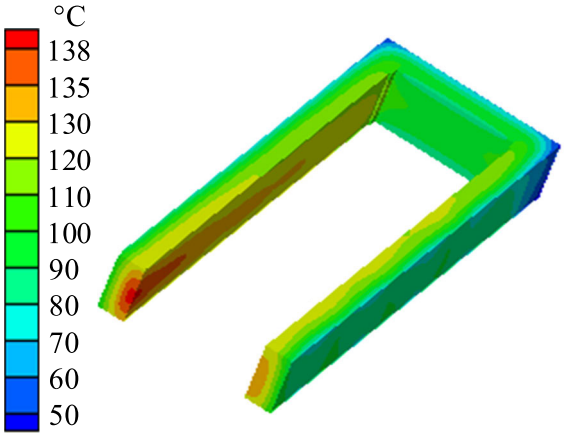

FIGURE 15. Temperature distribution of rotor excitation winding.

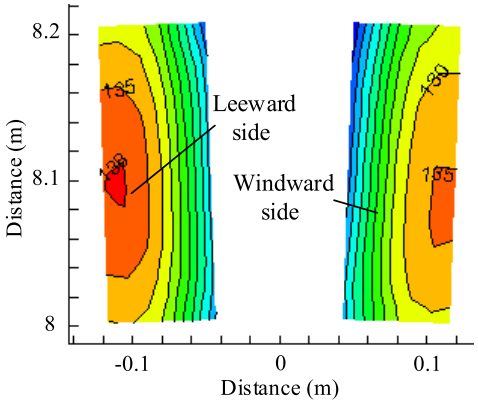

FIGURE 16. Isotherm of rotor excitation winding.

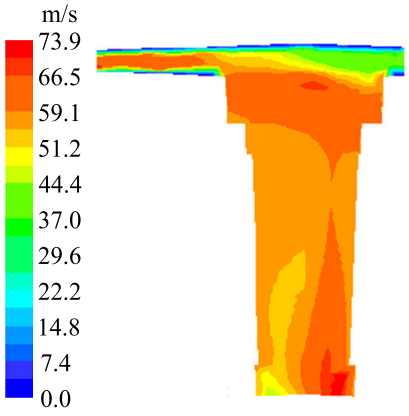

FIGURE 17. Fluid velocity distribution when the width of the rotor excitation winding increases by 5mm.

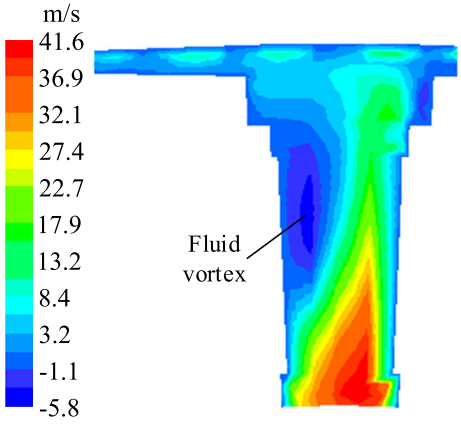

FIGURE 18. Radial fluid velocity distribution when the width of the rotor excitation winding increases by 5mm.

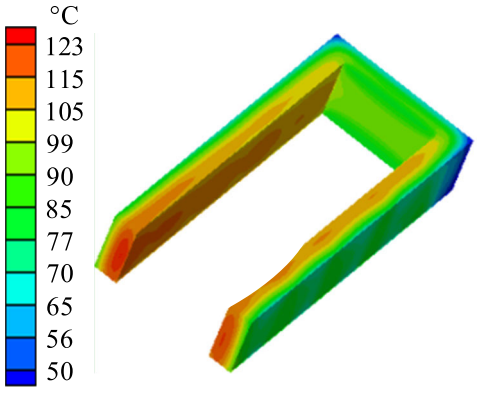

FIGURE 19. Temperature distribution of rotor excitation winding.

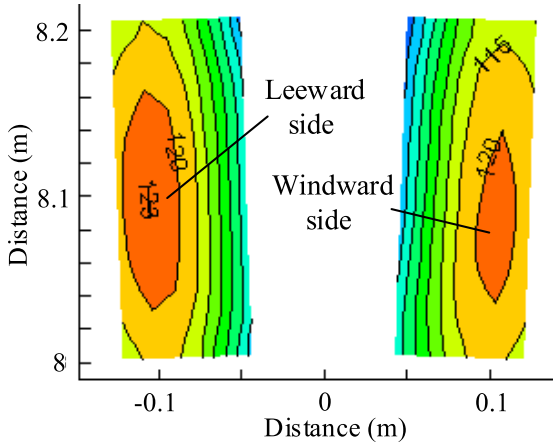

FIGURE 20. Isotherm of rotor excitation winding.

C. INFLUENCE OF THE WIDTH OF THE ROTOR EXCITATION WINDING ON THE FLUID VELOCITY AND TEMPERATURE IN THE ROTOR REGION OF HYDROGENERATOR

In order to study influence of the width of the rotor excitation winding on the fluid velocity and temperature distribution in the rotor region of hydrogenerator, the width of the rotor excitation winding increases by 5mm or decreases by 5mm when the current of the rotor excitation winding remains unchanged. Figs. 17 and 18 show the distribution of fluid velocity and radial fluid velocity between the rotor magnetic poles when the width of the rotor excitation winding increases by 5mm. It can be seen from Fig. 17 that the highest fluid velocity is 73.9m/s in this section. Fig. 18 shows the highest radial fluid velocity is 41.6m/s in this section when the width of the rotor excitation winding increases by 5mm.

The heat density of the rotor excitation winding reduces as the width of the rotor excitation winding increases. Fig. 19 shows the temperature distribution of rotor excitation

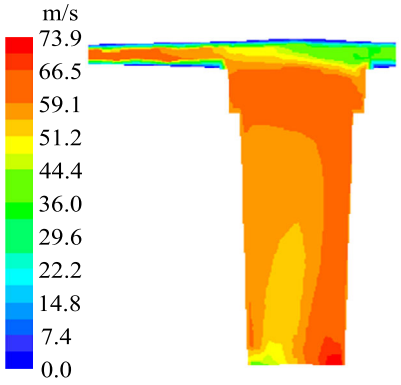

FIGURE 21. Fluid velocity distribution when the width of the rotor excitation winding increases by 5mm.

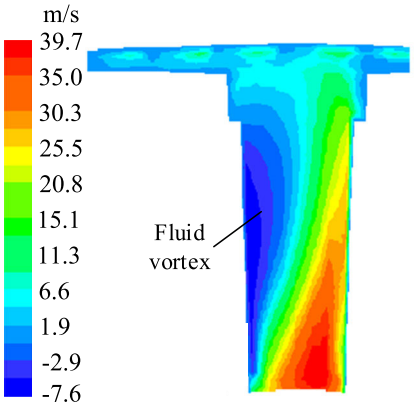

FIGURE 22. Radial fluid velocity distribution when the width of the rotor excitation winding increases by 5mm.

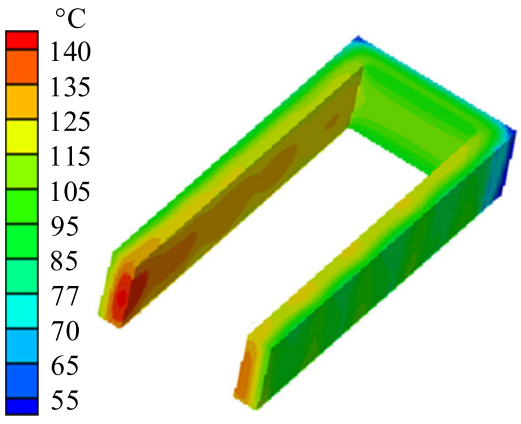

FIGURE 23. Temperature distribution of rotor excitation winding.

winding when the width of the rotor excitation winding increases by 5mm. The highest temperature of the rotor excitation winding is 123°C and appears on the leeward side. It is 9°C lower than that of the rotor excitation winding on the leeward side under the original structure. Fig. 20 gives the isotherm of rotor excitation winding. The temperature difference of rotor excitation winding on the leeward side and on the windward side is 3°C.

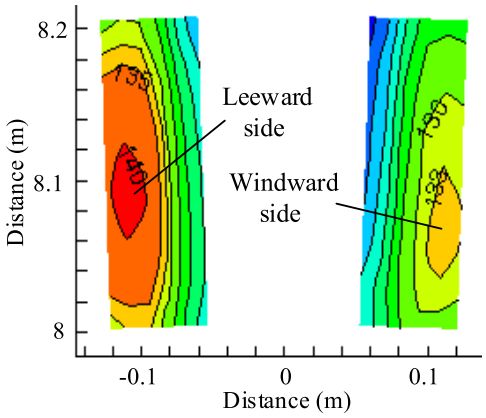

FIGURE 24. Isotherm of rotor excitation winding.

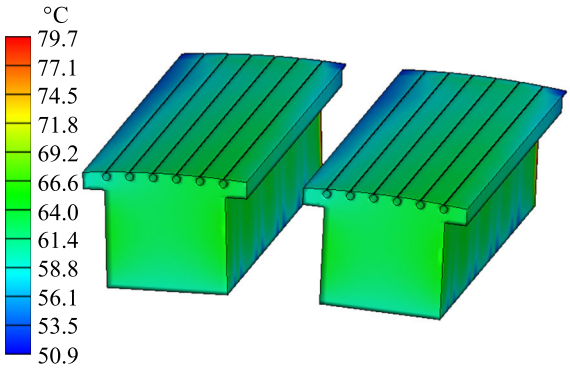

FIGURE 25. Temperature distribution of rotor pole body.

Figs. 21 and 22 show the distribution of fluid velocity and radial fluid velocity between the rotor magnetic poles when the width of the rotor excitation winding decreases by 5mm. Fig. 21 shows that the highest fluid velocity is 73.9m/s in this section. Fig. 22 shows the highest radial fluid velocity is 39.7m/s in this section when the width of the rotor excitation winding decreases by 5mm.

Fig. 23 shows the temperature distribution of rotor excitation winding when the width of the rotor excitation winding decreases by 5mm. The highest temperature of the rotor excitation winding is 140°C and appears on the leeward side. It is 8°C higher than that of the rotor excitation winding on the leeward side under the original structure. The highest temperature of the rotor excitation winding is 133°C on the windward side. It is 10°C higher than that of the rotor excitation winding on the windward side under the original structure. Fig. 24 gives the isotherm of rotor excitation winding. The temperature difference of rotor excitation winding on the leeward side and on the windward side is 7°C.

Figs. 25 and 26 give temperature distribution of rotor pole body and rotor pole body insulation. The highest temperature of rotor pole body and rotor pole body insulation is 79.7°C and 115.4°C when the width of the rotor excitation winding increases by 5mm, respectively. The temperature difference of the highest temperature and the lowest temperature of rotor pole body is 28.8°C.

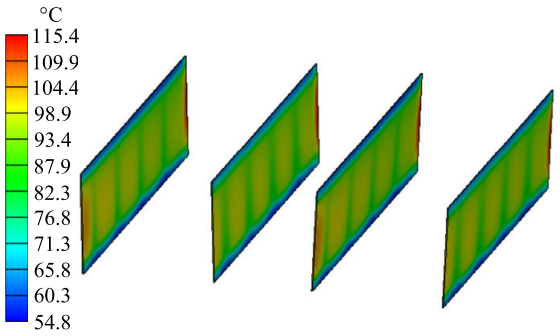

FIGURE 26. Temperature distribution of rotor pole body insulation.

TABLE 3. Measured value and calculated result of the temperature of rotor excitation winding.

Rotor excitation winding	Measured values	Calculated results
Temperature (°C)	108.6	106

D. PROTOTYPE EXPERIMENT AND VERIFICATION

In order to verify the accuracy of calculated results, the temperature of the rotor excitation winding is measured online at the power plant under the original structure. The measured average temperature of the rotor excitation winding is 108.6°C. The measured value and calculated result of the temperature of rotor excitation winding is shown in Table 3. It can be seen that the calculated result is close to the measured value. It shows the calculated result is accuracy and the calculated method is reliable.

V. CONCLUSION

In this paper, influence of the structures of the rotor support plate, rotor pole body insulation, and rotor excitation winding on the fluid flow between the rotor magnetic poles and temperature of the rotor parts is studied in the rotor region of hydrogenerator. Some conclusions are obtained as follows:

1. The highest fluid velocity is 76.9m/s when the width of the rotor support plate reduces by 5mm. The highest temperature of the rotor excitation winding is 133°C and appears on the leeward side. It is 1°C higher than that of the rotor excitation winding on the leeward side under the original structure. The highest temperature of rotor pole body and rotor pole body insulation is 75.5°C and 107°C when the width of the rotor support plate reduces by 5mm, respectively.

2. The highest temperature of the rotor excitation winding is 138°C and appears on the leeward side when the thickness of rotor pole body insulation increases by 5mm. It is 6°C higher than that of the rotor excitation winding on the leeward side under the original structure. The highest temperature of the rotor excitation winding is 135°C on the windward side. It is 12°C higher than that of the rotor excitation winding on the windward side under the original structure. The temperature difference of rotor excitation winding on the leeward side and on the windward side is 3°C.

3. The highest temperature of the rotor excitation winding is 123°C and appears on the leeward side when the width of the rotor excitation winding increases by 5mm. It is 9°C lower than that of the rotor excitation winding on the leeward side under the original structure. When the width of the rotor excitation winding decreases by 5mm, the highest temperature of the rotor excitation winding is 140°C and appears on the leeward side. It is 8°C higher than that of the rotor excitation winding on the leeward side under the original structure. The highest temperature of the rotor excitation winding is 133°C on the windward side.

REFERENCES

[1] M. W. Meiswinkel, A. Ebrahimi, C. Wohlers, and T. Neschitsch, "Transient Roebel bar force calculation in large salient-pole synchronous machines," *IEEE Access*, vol. 9, pp. 2266–2273, Dec. 2021.

[2] C. Carounagarane, T. R. Chelliah, and D. Khare, "Analysis on thermal behavior of large hydrogenerators operating with continuous overloads," *IEEE Trans. Ind. Appl.*, vol. 56, no. 2, pp. 1293–1305, Mar. 2020.

[3] T. Øyvang, J. K. Nøland, G. J. Hegglid, and B. Lie, "Online model-based thermal prediction for flexible control of an air-cooled hydrogenerator," *IEEE Trans. Ind. Electron.*, vol. 66, no. 8, pp. 6311–6320, Aug. 2019.

[4] H. C. Dirani, A. Merkhouf, B. Kedjar, A.-M. Giroux, and K. Al-Haddad, "Rotor interturn short circuit impact on large hydrogenerator magnetic quantities," *IEEE Trans. Ind. Appl.*, vol. 54, no. 4, pp. 3702–3711, Jul. 2018.

[5] M. Valavi, K. G. Jørstad, and A. Nysveen, "Electromagnetic analysis and electrical signature-based detection of rotor inter-turn faults in salient-pole synchronous machine," *IEEE Trans. Magn.*, vol. 54, no. 9, Sep. 2018, Art. no. 8104309.

[6] J. C. Akiror, P. Pillay, and A. Merkhouf, "Challenges in modeling of large synchronous machines," *IEEE Trans. Ind. Appl.*, vol. 54, no. 2, pp. 1652–1662, Apr. 2018.

[7] A. Z. Gbégbé, B. Rouached, J. C. M. Bergeron, and P. Viarouge, "Damper currents simulation of large hydro-generator using the combination of FEM and coupled circuits models," *IEEE Trans. Energy Convers.*, vol. 32, no. 4, pp. 1273–1283, Dec. 2017.

[8] M. Schrittwieser, O. Bíró, E. Farnleitner, and G. Kastner, "Analysis of temperature distribution in the stator of large synchronous machines considering heat conduction and heat convection," *IEEE Trans. Magn.*, vol. 51, no. 3, Mar. 2015, Art. no. 8101304.

[9] J. C. Akiror, A. Merkhouf, C. Hudon, and P. Pillay, "Consideration of design and operation on rotational flux density distributions in hydrogenerator stators," *IEEE Trans. Energy Convers.*, vol. 30, no. 4, pp. 1585–1594, Dec. 2015.

[10] G. Traxler-Samek, R. Zickermann, and A. Schwery, "Cooling airflow, losses, and temperatures in large air-cooled synchronous machines," *IEEE Trans. Ind. Electron.*, vol. 57, no. 1, pp. 172–180, Jan. 2010.

[11] W. Li, X. Zhang, S. Cheng, and J. Cao, "Thermal optimization for a HSPMG used for distributed generation systems," *IEEE Trans. Ind. Electron.*, vol. 60, no. 2, pp. 474–482, Feb. 2013.

[12] B. Dong, K. Wang, B. Han, and S. Zheng, "Thermal analysis and experimental validation of a 30 kW 60000 r/min high-speed permanent magnet motor with magnetic bearings," *IEEE Access*, vol. 7, pp. 92184–92192, Jul. 2019.

[13] P. S. Ghahfarokhi, A. Podgornovs, A. Kallaste, A. J. M. Cardoso, A. Belahcen, T. Vaimann, H. Tiismus, and B. Asad, "Opportunities and challenges of utilizing additive manufacturing approaches in thermal management of electrical machines," *IEEE Access*, vol. 9, pp. 36368–36381, 2021.

[14] P. S. Nasab, R. Perini, A. Di Gerlando, G. M. Foglia, and M. Moallem, "Analytical thermal model of natural-convection cooling in axial flux machines," *IEEE Trans. Ind. Electron.*, vol. 67, no. 4, pp. 2711–2721, Apr. 2020.

[15] J. Han, B. Ge, and W. Li, "Influence of magnetic permeability of the press plate on the loss and temperature of the end part in the end region of a turbogenerator," *IEEE Trans. Ind. Electron.*, vol. 66, no. 1, pp. 162–171, Jan. 2019.

[16] Z. Zhu, W. Zhang, Y. Li, and J. Guo, "Thermal analysis of axial permanent magnet flywheel machine based on equivalent thermal network method," *IEEE Access*, vol. 9, pp. 33181–33188, Feb. 2021.

[17] Z. Shah, M. Sheikholeslami, K. Ikramullah, and P. Kumam, "Simulation of entropy optimization and thermal behavior of nanofluid through the porous media," *Int. Commun. Heat Mass Transfer*, vol. 120, Jan. 2021, Art. no. 105039.
[18] Z. Shah, A. Dawar, and S. Islam, "Influence of brownian motion and thermophoresis parameters on silver-based di-hydrogen CNTs between two stretchable rotating disks," *Phys. Scripta*, vol. 96, no. 5, May 2021, Art. no. 055205.
[19] C. Zhang, L. Chen, X. Wang, and R. Tang, "Loss calculation and thermal analysis for high-speed permanent magnet synchronous machines," *IEEE Access*, vol. 8, pp. 92627–92636, May 2020.
[20] K. Bersch, S. Nuzzo, P. H. Connor, C. N. Eastwick, R. Rolston, and M. Galea, "Thermal and electromagnetic stator vent design optimisation for synchronous generators," *IEEE Trans. Energy Convers.*, vol. 36, no. 1, pp. 207–217, Mar. 2021.
[21] W. Tong, S. Wu, and R. Tang, "Research on the airflow and thermal performance in a large forced air-cooled permanent magnet synchronous machine," *IEEE Access*, vol. 7, pp. 162343–162352, Nov. 2019.
[22] S. Ding, M. Zhu, Y. Wang, and W. Liu, "Temperature rise effect of permanent magnet wind turbine in different field settings," *IEEE Access*, vol. 7, pp. 175324–175330, Aug. 2019.

HAN JICHAO was born in Harbin, China, in 1986. He received the B.S., M.S., and Ph.D. degrees in electrical machinery and appliance from the Harbin University of Science and Technology, Harbin, in 2010, 2013, and 2015, respectively. He is currently an Associate Professor with the Harbin University of Science and Technology. He is the author or coauthor of more than 20 refereed technical articles in IEEE transactions and IET proceedings, and holds more than 20 invention patents. His research interests include research on ventilation cooling, electromagnetics, fluids, and thermal analysis on large electrical generators, particularly in large turbogenerators.

LIU YUFEI was born in Harbin, China, in 1997. He received the B.S. degree in electrical engineering and automation from the Harbin University of Science and Technology, Harbin, in 2019, where he is currently pursuing the M.S. degree in electrical machinery and appliance. His research interests include research on electromagnetics and thermal analysis on electrical generator.

DONG JIECHEN was born in Anda, China, in 1997. He received the B.S. degree in electrical engineering and automation from the Harbin University of Science and Technology, Harbin, China, in 2020, where he is currently pursuing the M.S. degree in electrical machinery and appliance. His research interests include research on ventilation cooling, fluids, and thermal analysis on electrical generator.

SUN YUTIAN was born in 1963. He received the B.S. and M.S. degrees in electrical machinery and appliance from the Harbin University of Science and Technology, Harbin, China, in 1984 and 1987, respectively, and the Ph.D. degree in electrical machine from the Shenyang University of Technology, Shenyang, in 1998. He is currently the Deputy Chief Designer with the State Key Laboratory of Hydro-Power Equipment, Harbin Electric Machinery Company Ltd., and the Harbin Institute of Large Electrical Machinery. He is engaged in the design of large generator.

GE BAOJUN was born in 1960. He received the B.S. and M.S. degrees in electrical machinery and appliance from the Harbin University of Science and Technology, Harbin, China, in 1982 and 1985, respectively, and the Ph.D. degree in electrical machine and appliance from the Harbin Institute of Technology, Harbin, in 1999.

He is currently a Professor with the Harbin University of Science and Technology. He is the author or coauthor of more than 100 published refereed technical articles and four books. He is also the Head of the National High Quality Courses of Electrical Machinery. His research interests include new technology of large generator, electromechanical energy conversion, and coordinate theory of generators and power grids.

LI WEILI received the M.S. degree from the Harbin Institute of Electrical Technology, Harbin, China, in 1993, and the Ph.D. degree from the Russia Electric Power Research Institute, Saint Petersburg, Russia, in 1997.

He is currently a Professor with the Harbin University of Science and Technology. He is the author or coauthor of more than 200 published refereed technical articles and the holder of 22 patents. His research interests include synthesis physical field analyses on large electrical machines, renewable energy systems, and special electrical machines and associated control.